ISBN: 978-3-95450-249-3 ISSN: 2673-5350 doi: 10.18429/JACoW-IBIC2024-TUP13

DESIGN OF BEAM POSITION MONITOR OF WUHAN PHOTON SOURCE

Haoyu Dong, Zhengqiu Luo, Zhengzheng Liu†
Huazhong University of Science and Technology, Wuhan, China
Geng Wei, HaoHu Li, Wuhan University, Wuhan, China

Abstract

Wuhan Photon Source (WHPS), as a fourth-generation synchronous light source, imposes stringent requirements on the resolution and longitudinal coupling impedance of the Beam Position Monitor (BPM). To address the need for beam current monitoring in its 1.5 GeV diffraction-limited storage ring, an optimized design scheme for button BPM is proposed. Additionally, the structure of the BPM feedthrough is enhanced, and a detailed investigation into the impact of various materials on the longitudinal coupling impedance of the BPM is conducted. These findings serve as a valuable reference for the future design of similar BPM systems.

INTRODUCTION

WHPS utilizes a double-ring design [1], receiving full energy injection from a linear accelerator (LINAC). This configuration comprises a 180-meter-long low-energy diffraction-limited synchrotron radiation source operating at 1.5 GeV and a 927-meter-long fourth-generation medium-energy diffraction-limited synchrotron radiation source operating at 4.0 GeV. The overall schematic of the facility is illustrated in Fig. 1 [2].

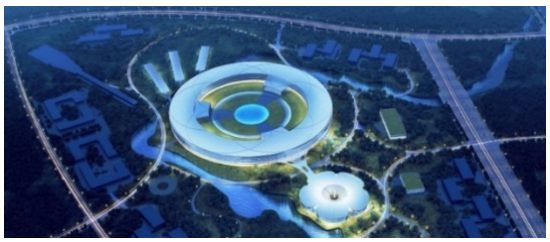

Figure 1: WHPS global schematic.

The fundamental design parameters of the WHPS are presented in Table 1 [3]. For the 1.5 GeV storage ring, as indicated in the Table 1, the beam bunch exhibits an RMS length of 5.4 mm, a beam current intensity of 500 mA, and operates at an RF frequency of 499.654 MHz, representing a short beam bunch characterized by a high repetition rate and substantial charge. Within the diffraction-limited storage ring light source, maintaining beam orbital stability at a sub-micrometer scale necessitates the provision of real-time and precise beam lateral position data by the beam position measurement system.

As the cornerstone of the beam position measurement system, the performance of the BPM significantly influences the overall measurement accuracy. In the realm of light sources founded on diffraction-limited storage rings, two primary types of BPM are employed for beam position monitoring: the stripline BPM, suitable for measuring short beam bunches with low charge, and the button BPM, more adept at measuring beam bunches with high charge and a rapid repetition rate. Consequently, the button BPM is better suited for determining the position of beams with high frequencies and currents within WHPS. Hence, this study aims to design a high-resolution button BPM tailored for the 1.5 GeV storage ring of WHPS. When the storage ring operates in SA mode, a position resolution of 0.2 μm is mandated. In FA mode, the required position resolution is 0.6 μm, while in TBT mode, a position resolution of 1 μm is necessary. These specifications serve as guidelines for the design of the electrode geometry.

Table 1: Major Physical Parameters of the WHPS

Parameter	Symbol	Value
Energy	E_{low}	1.5 GeV
Radio frequency	f_{RF}	499.654 MHz
Bunch length	$\sigma_{\mathrm{r\ ms.low}}$	5.4 mm
Current	$I_{avg.low}$	500 mA
Cyclotron frequency	$f_{acc.low}$	1665.5 kHz
Emittance	$\varepsilon_{\mathrm{low}}$	226.4 pm-rad

STORAGE RING BUTTON BPM DESIGN

The primary focus of the button BPM design lies in the feedthrough, with attention directed toward two key aspects: firstly, ensuring that the geometrical parameters of the button pickup electrode align with the position resolution requirements of the beam position measurement system across various operational modes of the storage ring; and secondly, optimizing the wakefield impedance. This optimization primarily involves the design of the structure and selection of materials for the coaxial section within the feedthrough.

BPM Electrode Design

The geometric parameters of the BPM pickup electrode, encompassing the button radius, button thickness, and button gap, play a pivotal role in determining the position measurement accuracy of the BPM system [4]. Drawing from the design expertise of BPMs utilized in prominent advanced light sources both domestically and internationally, as well as practical operational insights [5-7], the specific design choices for this study include a button radius of 3 mm, a button thickness of 2 mm, a button gap of 0.3 mm, and a position gain coefficient (k_i) of 11.5243 mm

† Corresponding author.
Email address：zzliu@hust.edu.cn.

ISBN: 978-3-95450-249-3 ISSN: 2673-5350 doi: 10.18429/JACoW-IBIC2024-TUP13

under these geometric parameters. The formula for the power of the electrode signal is:

$$P(\omega)=\frac{|I(\omega)|^2 R_0 r^4 \omega^2}{8R^2c^2\left[1+(\omega R_0 C_b)^2\right]}. \quad (1)$$

Here, R_0 represents the characteristic impedance, set at 50 Ω to ensure impedance matching. ω denotes the operating angular frequency, while the operational frequency, f, is specified as 499.6 MHz. The amplitude of the beam current at the operating angular frequency, corresponding to the target current of 500 mA, is denoted by I(ω). The speed of light is denoted by c, and C_b represents the electrode capacitance, determined as 1.175 pF based on the geometric parameters of the electrode in question. Additionally, r signifies the radius of the button. The induced signal power of the BPM electrodes, calculated using Eq. (1), amounts to -12.8 dB.

The noise power components are multifaceted, predominantly comprising thermal noise, noise stemming from cable attenuation during transmission, and other sources of noise. The formula for thermal noise is:

$$P_{noise}=4k_B T\Delta f. \quad (2)$$

Here, K_B denotes the Boltzmann constant. The absolute temperature T represents the environment's temperature where the BPM is situated, measured in Kelvin [K], and set at 300 K in this design. Δf stands for the bandwidth of the storage ring across various operational modes. Cable attenuation during signal transmission is a significant factor to consider. For this design, the chosen coaxial cable model is LMR-400, and its attenuation is approximately 7.5 dB.

Other noise factors primarily encompass the impact of insertion loss from patch cords, noise introduced by amplifiers and filters, and various additional elements, collectively denoted as N_{else} , typically approximated at 5 dB. Consequently, the signal-to-noise ratio (SNR) of the BPM signal is calculated using the formula:

$$\mathrm{SNR_{dB}}=10\times\log_{10}^{\left(\frac{P(\omega)}{P_{noise}}\right)}-N_{cable}-N_{else}. \quad (3)$$

The BPM position resolution is determined by the position gain coefficient and SNR, as calculated by the formula:

$$\sigma=k_i\cdot\frac{1}{\sqrt{SNR}}. \quad (4)$$

Taking into account the varying bandwidth of different operational modes within the storage ring, the resolution criteria for the TBT and FA modes are more stringent compared to the SA mode [7], as determined by Eq. (4). The position resolution of BPM in the TBT mode is 0.61 μm, while in the FA mode it is 0.19 μm, both meeting their respective resolution requirements.

BPM Wakefield Impedance Optimization

The wakefield impedance, a critical parameter in BPM operation, exhibits distinct sharp resonance peaks within its impedance spectrum. Higher peak values in this spectrum indicate a heightened interaction between the beam bunch and the vacuum environment, potentially resulting in various beam instabilities like beam bunch stretching and head-to-tail cluster instabilities [8]. Conversely, lower frequencies associated with these impedance peaks bring them closer to the BPM electronic operating frequency, risking interference with the pickup, transmission, and identification of BPM position signal. Hence, optimizing the wakefield impedance by minimizing peak impedance levels and ensuring that their corresponding frequencies remain sufficiently distant from the BPM electronic operating frequency is essential.

The feedthrough comprises essential components such as button electrode, an inner conductor (pin), a sealing ceramic window made of dielectric material, and housing. The wakefield impedance primarily stems from structural irregularities and impedance mismatches within the feedthrough. Previous studies have indicated that the wakefield impedance is predominantly influenced by the internal feedthrough structure, electrode material, geometric dimensions, and dielectric material [9]. To meet the demanding requirements of measurement performance and resolution, a set of electrode geometry values has been established. Therefore, the focus of wakefield impedance optimization in this study revolves around the internal structure of the feedthrough and the materials of the electrode and ceramic window.

Figure 2 illustrates the feedthrough substructure design of the WHPS before undergoing structural optimization. Initial optimizations involve integrating the inner conductor with the button to mitigate structural irregularities resulting from welding. Step electrode is added above the button electrode to ensure the precision of ceramic window welding while increasing the smoothness of structural transition. Chamfering the edges of the ceramic window and step button aims to reduce sharp edges within the coaxial structure, ensuring smoother transitions. Following structural enhancements, as depicted in Fig. 3, a simulation model of the WHPS button BPM is established in CST, with four feedthroughs equipped with button symmetrically mounted on the vacuum pipe.

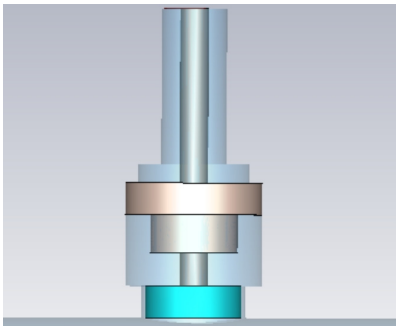

Figure 2: The design of the feedthrough substructure before optimization.

ISBN: 978-3-95450-249-3 ISSN: 2673-5350 doi: 10.18429/JACoW-IBIC2024-TUP13

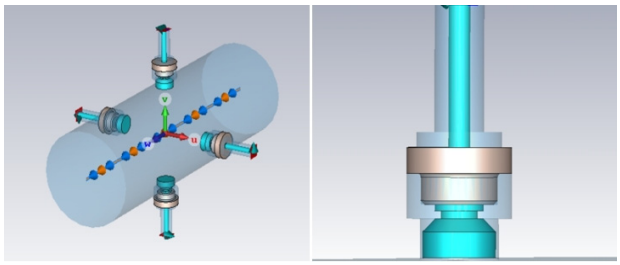

Figure 3: CST simulation model of WHPS button BPM after structural optimization.

Figure 4 delineates the wakefield impedance outcomes before and after structural optimization. In this context, curve Z1 depicts the wakefield impedance findings prior to structural refinement, while curve Z2 illustrates the impedance results post-optimization. The comparison reveals the presence of four notable impedance peaks within the 20 GHz range. Following structural optimization, the peak value of the highest impedance diminishes, and the frequencies of the second and fourth impedance peaks shift rearward. This change signifies that after optimization, the interaction between the beam bunch and the vacuum environment weakens, subsequently reducing the wakefield impedance's interference with the BPM position signal.

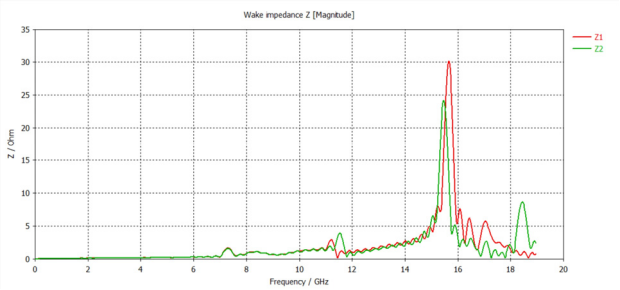

Figure 4: Wakefield impedance results before and after structural optimization.

The subsequent optimization of the wakefield impedance will focus on material selection, with a particular emphasis on the thermal performance of the chosen dielectric materials, as detailed in the forthcoming section. Commonly utilized electrode materials encompass titanium, molybdenum, and copper. However, due to copper's susceptibility to deformation under heat, leading to significant position measurement inaccuracies, titanium and molybdenum have been designated as the preferred electrode materials for this study. Additionally, aluminum nitride, alumina, and boron nitride have been selected as the dielectric materials under investigation.

The ceramic window component exhibits two distinct coaxial structures: the first structure comprises a small ceramic circle encircled by vacuum, creating a coaxial dielectric between the inner conductor and the outer wall; the second structure consists of a small vacuum circle surrounded by a larger ceramic circle, forming another coaxial dielectric between the inner conductor and the outer wall. The equivalent permittivity of these coaxial dielectric is calculated by the following equation:

$$\varepsilon_e = \frac{\varepsilon_{r1}\varepsilon_{r2}\ln\left(\frac{r_h}{r_p}\right)}{\varepsilon_{r1}\ln\left(\frac{r_h}{a}\right)+\varepsilon_{r2}\ln\left(\frac{a}{r_p}\right)}. \quad (5)$$

In the formula, r_p and r_h represent the radius of the inner conductor and the shell, respectively. And a is the radius of the interface between the two dielectrics, while ε_{r1} and ε_{r2} denote the relative permittivity of the inner and outer dielectrics, respectively. The theoretical formula for calculating the impedance of a coaxial conductor is as follows:

$$Z_0 = \ln(R/r)\times 60/\sqrt{\varepsilon_e}\ . \quad (6)$$

Here, R represents the radius of the outer conductor, and r signifies the radius of the inner conductor. When opting for various dielectric materials, the structural parameters for achieving a 50 Ω impedance match are first computed based on equations (5) and (6). These calculations serve as a foundation for structurally modeling simulations, offering theoretical insights into the process.

Once the modeling is finalized within the CST Particle Studio with accurate background materials and boundary conditions established, the wakefield solver is executed to derive the corresponding wakefield impedance outcomes. These results are depicted in Figs. 5 and Fig. 6.

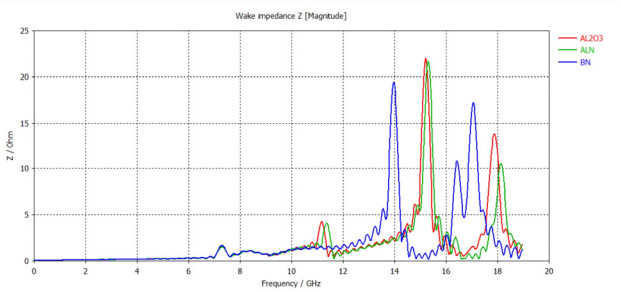

Figure 5: Simulation results of wakefield impedance using different dielectric materials when the electrode material is titanium.

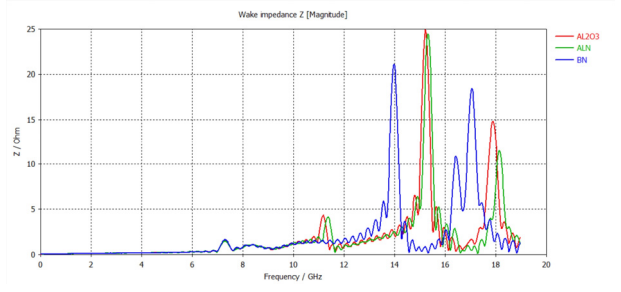

Figure 6: Simulation results of wakefield impedance using different dielectric materials when the electrode material is molybdenum.

Upon examination of the simulation outcomes presented in Fig. 5 and Fig. 6, a noticeable disparity emerges in the peak impedance of the wakefield when utilizing

ISBN: 978-3-95450-249-3 ISSN: 2673-5350 doi: 10.18429/JACoW-IBIC2024-TUP13

molybdenum versus titanium as the electrode material. Evidently, the wakefield impedance peaks are markedly higher when molybdenum is employed. Consequently, titanium is selected as the preferred electrode material. Furthermore, when boron nitride serves as the dielectric material, the frequencies corresponding to the two highest impedance peaks exhibit a significant forward shift compared to other materials. Additionally, an impedance peak is situated between these two prominent peaks, posing interference with the position signal. Consequently, greater emphasis is placed on alumina and aluminum nitride as potential dielectric materials. The subsequent section will focus on utilizing thermal simulation results to determine the dielectric material for the ultimate optimized design.

THERMAL ANALYSIS OF BPM

When the pick-up electrode of the BPM captures the beam position signal, power is inevitably deposited in certain structures due to the presence of wakefield impedance. This deposited power is difficult to dissipate and ultimately transforms into thermal energy, resulting in localized temperature rises within the BPM. If the overall heat dissipation capacity of the BPM proves inadequate, this thermal energy can lead to structural deformations, thereby compromising the BPM measurement accuracy and potentially endangering operational safety. Hence, thermal simulation stands as a crucial facet in button BPM design. The BPM thermal simulation model is established within the CST Mphysics Studio, exemplified in Fig. 7.

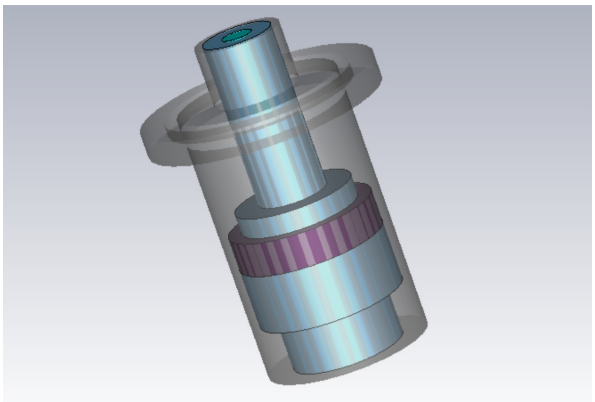

Figure 7: Thermal simulation model of button BPM.

The correlation analysis indicates that the power deposition within the ceramic section significantly surpasses that in other regions, warranting the designation of the ceramic section as the primary heat source [10]. To ensure a comprehensive simulation, the thermal power is rigorously fixed at 1 W. Once the boundary conditions and background materials are accurately configured, the thermal simulation can be initiated.

Titanium has been chosen as the electrode material, and for the thermal simulation analysis, different dielectric materials have been selected. The ensuing results of this analysis are depicted in Fig. 8.

Analysis of Fig. 8 reveals that due to the superior thermal conductivity of aluminum nitride, enhanced heat dissipation capability is achieved. Consequently, the BPM utilizing aluminum nitride as the dielectric material exhibits a comparatively minor temperature differential spanning from the base of the electrode to the apex of the inner conductor. This configuration mitigates the risk of temperature escalation and structural deformation in various components. Integrating this thermal analysis with the prior examination of wakefield impedance, the ultimate optimized design elects titanium as the electrode material and aluminum nitride as the dielectric material.

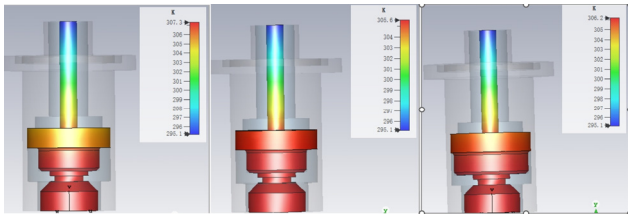

Figure 8: BPM thermal simulation results of alumina (left), aluminum nitride (medium), boron nitride (right) as dielectric materials.

CONCLUSION

In this research, a refined design approach is introduced for the button BPM within the 1.5 GeV storage ring of the Wuhan Photon Source. The optimization primarily focuses on the structure and material of the button BPM feedthrough. The investigation delves deeply into the impact of diverse electrode materials, dielectric materials, and their respective configurations on wakefield impedance. Following meticulous analysis, titanium emerges as the preferred electrode material. Subsequently, through comprehensive thermal simulations, aluminum nitride is identified as the optimal dielectric material.

The overarching principles guiding this optimized design endeavor aim to minimize abrupt structural changes within the feedthrough, enhance the smoothness of structural transition, and select electrode and dielectric materials that effectively optimize wakefield impedance and heat dissipation. Noteworthy is the recognition that structural modifications to the button electrode itself can influence both wakefield impedance and overall thermal dissipation within the BPM. This realization underscores the ongoing need for further exploration and optimization in the realm of structural and shape adjustments to optimize wakefield impedance and thermal performance in the BPM.

REFERENCES

[1] H. H. Li *et al.*, "Project of Wuhan Photon Source", in *Proc. IPAC'21,* Campinas, SP, Brazil, May. 2021, pp. 346-349. doi:10.18429/JACoW-IPAC2021-MOPAB092

[2] Z. Luo, "Study on button BPM for fourth-generation light source diffraction-limit storage ring", Master's thesis, Nuclear science and technology, Huazhong University of Science and Technology, Wuhan, China, 2023. doi:10.27157/d.cnki.ghzku.2023.004389

[3] H. H. Li *et al.*, "Accelerator system of Wuhan Light Source phase I project", *Atomic Energy Sci. Tech.*, vol. 56, no. 9,

ISBN: 978-3-95450-249-3 ISSN: 2673-5350 doi: 10.18429/JACoW-IBIC2024-TUP13

pp. 1860-1868, 2022.
doi:10.7538/yzk.2022.youxian.0360

[4] Forck P *et al*., "Beam Position Monitors", in *Course on Beam Diagnostics*, Dourdan, France, pp. 187-228, 2008. doi:10.5170/CERN-2009-005.187

[5] P. F. Tavares *et al.,* "The MAX IV storage ring project", *J. synchrotron Radiat*., vol. 21, no. 5, pp. 862-877, Aug. 2014. doi:10.1107/S1600577514011503

[6] N. Milas *et al.*, "Sirius Diagnostic Beamlines", in *Proc. IPAC'14*, Dresden, Germany, Jun. 2014, pp. 3427-3429. doi:10.18429/JACoW-IPAC2014-THPME082

[7] J. He *et al*., "Beam position monitor design for the high energy photon source", *Meas. Sci. Tech.*, vol. 33, no. 11, p. 115106, 2022. doi:10.1088/1361-6501/ac8277

[8] R. Yuan, "Study on beam position measurement and its application in BEPCII", Doctoral thesis, Accelerator Center, China, 2004. http://ir.ihep.ac.cn//handle/311005/113574

[9] J. He *et al*., "Design and fabrication of button-style beam position monitors for the HEPS synchrotron light facility", *Nucl. Sci. Tech.*, vol. 33, no. 11, Nov. 2022. doi:10.1007/s41365-022-01126-7

[10] G. Zhao *et al*., "Thermal deformation simulation of BPM button electrode beam load for Shanghai Synchrotron Radiation Facility", *Nucl. Tech.*, vol. 37, no. 5, p. 050101, May. 2014. http://ir.sinap.ac.cn/handle/331007/14673